THE JOURNAL OF BIOLOGICAL CHEMISTRY VOL. 285, NO. 40, pp. 30814–30824, October 1, 2010

ZFP423 Coordinates Notch and Bone Morphogenetic Protein Signaling, Selectively Up-regulating *Hes5* Gene Expression*[S]

Received for publication, June 14, 2010 Published, JBC Papers in Press, June 14, 2010, DOI 10.1074/jbc.M110.142869

Giacomo Masserdotti[‡§1,2], Aurora Badaloni[‡1], Yangsook Song Green[¶], Laura Croci[‡], Valeria Barili[‡§], Giorgio Bergamini[‡§], Monica L. Vetter[¶], and G. Giacomo Consalez[§3]

From the [‡]Division of Neuroscience, San Raffaele Scientific Institute, 20132 Milan, Italy, the [§]Università Vita-Salute San Raffaele, 20132 Milan, Italy, and the [¶]Department of Neurobiology and Anatomy, University of Utah, Salt Lake City, Utah 84132

Zinc finger protein 423 encodes a 30 Zn-finger transcription factor involved in cerebellar and olfactory development. ZFP423 is a known interactor of SMAD1-SMAD4 and of Collier/Olf-1/EBF proteins, and acts as a modifier of retinoic acid-induced differentiation. In the present article, we show that ZFP423 interacts with the Notch1 intracellular domain in mammalian cell lines and in *Xenopus* neurula embryos, to activate the expression of the Notch1 target *Hes5*/*ESR1*. This effect is antagonized by EBF transcription factors, both in cultured cells and in *Xenopus* embryos, and amplified *in vitro* by BMP4, suggesting that ZFP423 acts to integrate BMP and Notch signaling, selectively promoting their convergence onto the *Hes5* gene promoter.

A small set of regulatory factors, mostly secreted or surface molecules, modulates neural development, from neural induction through synaptogenesis. Morphogens, acting instructively, permissively, or through inhibitory interactions, control various aspects of neurogenesis, eliciting different responses in target cells, dependent upon their evolving windows of competence. The integrated effects of various morphogens regulate a range of developmental switches, controlling, among other aspects, regional identity, fate determination, and the timing of neuronal commitment and differentiation. Although the activities of extracellular factors have been intensively studied, many of their cell-intrinsic effectors have yet to be discovered and characterized.

The Notch pathway exerts regulatory activities in a diverse array of developmental contexts (reviewed in Refs. 1, 2). In neurogenesis, Notch signaling suppresses the neurogenetic cascade, which is promoted and sustained by proneural basic helix-loop-helix (bHLH) transcription factors. When the Notch single pass receptor is bound by the Delta or Jagged/Serrate family of transmembrane ligands expressed by adjacent cells, the Notch intracellular domain (NICD)[4] is cleaved proteolytically (3, 4) and translocates into the nucleus. There, it interacts with the DNA-binding protein CSL$^{CBF1/Su(H)/LAG-1}$ (5), displacing a co-repressor complex (6) and recruiting a transcriptional activation complex (7–9). This leads to the transcription of various immediate target genes, including *Drosophila enhancer of Split*, and its vertebrate homologs *Hairy*, *Hes1*, and *Hes5* (10–12). These genes encode transcriptional repressors of the basic helix-loop-helix family, which act as inhibitors of neuronal differentiation. In the developing nervous system, *Hes1*, *Hes5* double mutants feature a loss of mitotic progenitors and a massive premature differentiation, particularly in the dorsal neural tube (13).

Whereas this pathway effectively delays neuronal commitment and differentiation, it also promotes diversity in neuronal development by actively preserving a pool of uncommitted and mitotic neural progenitors, sustaining the birth of successive waves of distinct neuronal and glial types (reviewed in Ref. 14). To perform this broad array of modulatory effects at different developmental stages and in distinct morphogenetic domains, the Notch signaling cascade is tightly regulated, from the cell surface to the nucleus (reviewed in Refs. 15, 16).

The *Zfp423* gene is expressed alongside the dorsal midline of the embryonic mouse neural tube, at the border with the roof plate, particularly in the hindbrain and cerebellum (17). The roof plate provides critical signals for cerebellar development (18). The gene encodes a 30 Zn-finger domain nuclear protein involved in cerebellar and olfactory development. Interestingly, *Zfp423* null mice develop a profound hypoplasia of the cerebellar vermis (19–21), reminiscent of the Dandy-Walker malformation (reviewed in Ref. 22), and a premature differentiation of olfactory neuron progenitors (23), although the underlying molecular mechanisms remain unclarified.

ZFP423 is known to interact with the SMAD1-SMAD4 complex, which transduces bone morphogenetic protein (BMP2/4/7) signaling (reviewed in Ref. 24) into the nucleus, up-regulating *Xvent2* transcription in *Xenopus laevis* gastrulae and mammalian cells (25). However, no information is available to date as to the functional significance (if any) of the interaction

* This work was supported, in whole or in part, by National Institutes of Health Grant EY012274 (to M. L. V.). This work was also supported by the EU consortium contract EuroSyStem (to G. G. C.) and the Fondazione CARIPLO (Network Operativo per la Biomedicina di Eccellenza in Lombardia), from the Italian Ministry of University and Research (MIUR-PRIN 2007).

[S] The on-line version of this article (available at http://www.jbc.org) contains supplemental Figs. S1 and S2.

[1] Both authors contributed equally to this work.

[2] Supported by a Ph.D. fellowship provided by the San Raffaele Scientific Institute.

[3] To whom correspondence should be addressed: Division of Neuroscience, San Raffaele Scientific Institute, Via Olgettina 58, 20132 Milano, Italy. Fax: +39-02-2643-5283; E-mail: g.consalez@hsr.it.

[4] The abbreviations used are: NICD, Notch intracellular domain; RL, rhombic lip; BMP, bone morphogenetic protein; BRE, BMP-responsive element; COE, Collier/Olf-1/EBF; EBF, Early B-cell factor; N^{act}, constitutively active *Xenopus* Notch; RTqPCR, reverse transcription and quantitative polymerase chain reaction; miRNA, microRNA; VZ, ventricular zone; ZBS, Zfp423 binding site; ZFP423, zinc finger protein 423.

of ZFP423 and receptor-dependent SMADs in mammalian neural development.

ZFP423 has also been found to complex with EBF^{COE} proteins (26, 27). EBF^{COE} TFs are important players in the context of neuronal differentiation and migration (28–31), olfactory neurogenesis (32–34), cerebellar PC migration, and survival (35) (68) and cerebellar cortical patterning (35, 36). Finally, a recent article described the role of ZFP423 as a modifier of retinoic acid-induced differentiation (37). Thus, ZFP423 is poised to interact with multiple signaling pathways and transcriptional effectors, likely integrating their function during development.

In the present work, we analyze some of the functional and molecular interactions established by ZFP423 *in vitro* and *in vivo*. We demonstrate that ZFP423 interacts functionally and molecularly with the NICD in mammalian cell lines and in *Xenopus* neurula embryos, to activate the expression of the Notch target *Hes5*/*ESR1*. A small proximal region of the *Hes5* promoter is sufficient to reproduce this cooperation *in vitro*. This effect is enhanced in BMP4 treated cells. By triggering *Hes5* expression and by modulating BMP signaling cell autonomously, ZFP423 may help maintain a pool of *Hes5* positive neurogenic progenitors in the developing neural tube.

EXPERIMENTAL PROCEDURES

Animal Care—All experiments described in this report were conducted in agreement with the stipulations of the San Raffaele Scientific Institute Animal Care and Use Committee, and the University of Utah Institutional Animal Care and Use Committee guidelines.

Tissue Preparation—Pregnant mice were anesthetized with Avertin (Sigma). For *in situ* hybridization on sagittal sections, embryos were fixed overnight by immersion with 4% PFA, cryoprotected in 30% sucrose overnight, embedded in OCT (Bioptica), and stored at −80 °C, before sectioning on a cryotome (20 μm). For whole mount *in situ* hydridization and whole mount LacZ staining embryos were fixed with 4% PFA 6 h or 10 min, respectively. *Zfp423* expression at embryonic day 10.5 was re-examined by LacZ staining using a transgenic line obtained from the German Genetrap Consortium (ID: W008G09, 38) carrying a LacZ gene inserted by gene trapping within the *Zfp423* gene. LacZ staining was performed as described (35).

Xenopus Embryo Microinjection—Mouse *Zfp423* from pCDNA3-*Zfp423* was subcloned into the pCS2+ expression vector and used to make capped mRNA *in vitro* using the Message mMachine kit (Ambion). Also, the following constructs were used as DNA templates to make capped mRNA : pCS2+X-Delta^{stu} (67), pCS2+MT-XotchΔE (referred to here as N^{act}) (39), pCS2+Xebf2 (29), pCS2+Xebf3 (29), pCS2+nβgal (40), and pCS2+GFP (41). The full length *Xenopus Zfp423* (XZfp423) cDNA including part of 5′-UTR was acquired by 5′-RACE (Roche) using the sequence of image clone 6636947, and then by RT-PCR with Superscript II Reverse Transcriptase (Invitrogen) and PfuUltraII fusion HS DNA polymerase (Stratagene) (GenBank™ Accession No. GQ421283). Control morpholino: the sequence of our XZfp423 morpholino (Gene Tools) is TCCACTGTACCTCAAAACTAACCCC, which is complementary to nucleotides −26 to −2. mRNA and morpholino were injected into one blastomere of 2-cell stage embryos in the following amounts: *Zfp423* (1 ng for single injection and co-injection with *Delta^{stu}*, 600 pg for co-injection with *XotchΔE*), *Delta^{stu}* (400 pg), *XotchΔE* (100 pg), *Xebf2* (100 pg), *Xebf3* (100 pg), *nβgal* (50 pg), and *XZfp423* morpholino (30 ng). mRNA was injected into one dorsal blastomere of 16-cell stage embryos in the following amounts : *Zfp423* (300 pg) and *Gfp* (200 pg). mRNA for *nβgal* or *Gfp* was co-injected into all embryos as a tracer. Embryos were grown until neural plate stages (42) and fixed in MEMFA for 30 min (43). X-Gal staining was performed on the embryos injected with nβgal as described (44). GFP-expressing embryos were sorted under fluorescence based on which side was the injected side and fixed for 30 more minutes.

In Situ Hybridization—For whole mount *in situ* hybridizations of *Xenopus* embryos, the following constructs were used to generate antisense RNA probes : pCMV-sport6-XZfp423 (Image clone 6636947, ATCC), pBS-ESR1 (45), pBS-Hairy1 (46), and pBS-Nrarp (47). For mouse experiments, digoxygenin-labeled riboprobes were transcribed from plasmids containing *Hes1*, *Hes5*, and *Zfp423* cDNAs. Antisense RNA probes were generated *in vitro* using T7 or T3 RNA polymerase (Roche) and labeled with digoxigeninin-11-UTP (Roche). *In situ* hybridizations of whole-mount mouse embryos and embryonic sections were performed as described (35).

Cell Culture and DNA Transfection—The P19 cell line was maintained in MEM-α (Invitrogen) supplemented with 10% FBS (Invitrogen). The C2C12 myoblastic cells (American Type Culture Collection), COS7 and HEK293 cells were maintained in Dulbecco's modified Eagle's medium (DMEM) supplemented with 10% fetal bovine serum (FBS, EuroClone). P19, HEK293, and COS7 cells were transfected with Lipofectamine2000 according to the manufacturer's instructions (Invitrogen). P19 cells were grown in MEM-α medium (Invitrogen), 5% FBS, and neuralized with 10^{-6} M retinoic acid (Sigma) treatment for 24 h. C2C12 cells were transfected using Lipofectamine2000 and Plus reagent, according to the manufacturer's instructions (Invitrogen), and treated with 100 ng/ml BMP4 (R&D Systems) when specified.

Plasmids and Constructs—To generate pCDNA3–6Myc-ZFP423, we subcloned ZFP423 from pXY-ZFP423 (RZPD, IRAK MGC full-length cDNA, clone 961, Berlin, Germany), in pC2 + 6Myc. 6Myc-ZFP423 was excised and cloned into pCDNA3.1 vector (Clontech). pCDNA3-Flag-Notch-Intracellular-Domain (Flag-NICD) was a kind gift of Georg Feger (Serono). 1 kb and smaller fragment of the *Hes5* promoter were amplified from wild-type mouse genome, cloned into pBluescript SK and sequenced. The fragments were subcloned into the pGL3 vector (Promega). To generate pCDNA3-6myc-ZFP423Δ9–20, pCDNA3–6myc-ZFP423 was digested with the enzymes SacI and PvuII and the fragment (1381 bps) was cloned into pBluescript SK, previously opened with PvuII. A second fragment (2120 bps) obtained from pCDNA3–6myc-ZFP423 by SacI-SacII digestion and blunt, was cloned downstream of the first fragment in pBKS. 6myc-ZFP423Δ9–20 was excised with the enzymes HindIII-NotI and subcloned into pCDNA3.1 (Invitrogen).

RT-PCR—Total RNA was extracted with RNeasy MicroKit (Qiagen), according to the manufacturer's instructions. 1–1.5 μg of total RNA was retrotranscribed using first strand cDNA MMLV-Retrotranscriptase (Invitrogen) and random primers. Each cDNA was diluted 1:10, and 3 μl was used for each real-time reaction. mRNA quantitation was performed with LightCycler480 SYBR Green I Master Mix (Roche) on a LightCycler480 instrument (Roche) following the manufacturer's protocol.

The following primers were used: *Gapdh* (48); *Hes5*, *Hes1* (49); *Blbp* (50); *Zfp423* (25); flagNICD F: 5′-ATGGACTACAAAGACGATGAC, flagNICD R: 5′-CAAACCGGAACTTCTTGGTC.

RNA Interference—Single-stranded DNA oligos encoding the pre-miRNAs were annealed according to the manufacturer's instructions (Invitrogen). Pre-miRNA double-stranded oligos were cloned in pCDNA^{TM}6.2-GW/-EmGFP-miR vector (Invitrogen). A pre-miRNA containing a non-targeting sequence (Invitrogen) was used as a negative control. The pre-miRNAs were transfected via Lipofectamine2000 (Invitrogen) according to the manufacturer's instructions. To test the efficacy of the pre-miRNA, HEK293 cells were transfected with pcDNA3–6Myc-ZFP423 and either a non-targeting pre-miRNA or ZFP423-specific pre-miRNA vector, and cell lysates were analyzed via Western blot. Among the specific pre-miRNA tested, we selected the most effective one in abolishing protein expression. Transfected P19 cells were sorted for GFP expression and lysed for RNA extraction with RNeasy MicroKit (Qiagen), according to the manufacturer's instructions.

Coating Assay—To generate a soluble form of Notch1 ligand, 293T cells grown in a 10-cm Petri dish were transfected using Fugene HD (Roche), according to the manufacturer's instructions, with either 5 μg of Fc-TRAIL-Receptor 4 (Fc-control) or 5 μg of Fc-Jagged1 expression plasmids (Courtesy of Tom Kadesch, 51) After 48 h, the growth medium was collected and filtered through a 0.45-μm syringe filter. Fc-TRAIL-R4 or Fc-Delta4 fusion protein was immobilized by incubating polystyrene plates for 2 h at room temperature with 10 μg/ml rabbit anti-human IgG Fc antibody (Jackson ImmunoResearch Laboratories), and then incubated for 2 h with respective filtered supernatant. The pre-miRNAs were transfected in P19 cells via Lipofectamine 2000. After 48 h, the cells were splitted and grown for 24 h on plates coated with Fc-TRAIL-R4 (control) or Fc-Jagged1. Transfected P19 cells were sorted for GFP expression, and RNA was extracted with RNeasy MiniKit, according to the manufacturer's instructions.

Promoter Reporter Assays—The day before transfection, C2C12 cells were plated in 12-well plates and grown in DMEM supplemented with 10% FBS. Luciferase assays were carried out 24 h after transfection using Dual Luciferase Assay kit according to the manufacturer's instructions (Promega). Each result is the average of three independent measurements, and each experiment was repeated at least three times.

Chromatin Immunoprecipitation (ChIP)—P19 cells (2×10^6) were treated with 1% paraformaldehyde in 1× PBS by rotation for 10 min at room temperature. Fixation was stopped by addition of glycine to a final concentration of 125 mM. Cells were washed two times in 1× PBS and centrifuged at 2,000 rpm for 2 min. The pellet was resuspended in lysis buffer (5 mM PIPES, pH 8, 85 mM KCl, 0.5% Nonidet P-40, and protease inhibitors mixture) and incubated on ice for 10 min. After centrifugation at 4,000 rpm for 5 min at 4 °C, the pellet was resuspended in sonication buffer (50 mM Tris-HCl pH 8, 10 mM EDTA pH 8, 0.1% SDS, and protease inhibitors mixture). Sonication was performed five times with 20-s pulses using a microprobe at 40% output. Equal amounts of chromatin, precleared with blocked protein A-Sepharose (GE Healthcare), were incubated by overnight rotation with rabbit anti-OAZ (ZFP423) antibody (5 μg, H-105, Santa Cruz Biotechnology). Protein A-Sepharose was added to each sample and incubated at 4 °C with rotation for 3 h. Beads were spun at 14,000 rpm for 5 min, washed 6–8 times with wash buffer (10 mM Tris-HCl, pH 8, 0.5 mM EGTA, 1 mM EDTA, 140 mM NaCl, 1% Triton X-100, 0.1% SDS, 0.1% sodium deoxycholate), and eluted with 1% SDS in 50 mM $NaHCO_3$. Bound fractions were de-cross-linked by adding 200 mM NaCl and by incubation at 65 °C for 6–8 h. De-cross-linked samples were treated with RNase (0.03 mg/ml) and proteinase K (0.3 mg/ml) at 55 °C for 2 h. DNA was precipitated with 2.5 volumes of absolute ethanol and purified using Qiagen PCR Purification kit (Qiagen). Cross-link-reversed chromatin was used as a PCR control. For qPCR, each primer pair was assessed for amplification efficiency on serial dilutions of genomic DNA. PCR primer sequences: *Hes5* promoter (b), F: 5′-TTCCCACAGCCCGGACATT; R: 5′-GCGCACGCTAAATTGCCTGTGAAT; *Hes5* sequence a, F: 5′-TCAACTACTGTCCCTTCGCCCAGA; R: 5′- GGATTGGAGTCCTCTAGTTTGCCT; *Hes 5* sequence c: F: 5′-CTTGGTCATGTGGGAGAACA; R: 5′-GGCTGCTAAGGACAGACGAG; *Hes5* sequence d: F: 5′-TAGCTTACCACAGGAGCAGCAGAA; R: 5′-ACCCAGCAACTTCAGTCCCTGTAA; *Mrps15* (mitochondrial ribosomal protein S15), F: 5′-CTGGGACATAGTGGGTGCTT; R: 5′-GAGCCTAGAGATGGGCTGTG.

Immunoprecipitation and Western Blots—All biochemical procedures were conducted as described (52). In particular, COS7 and HEK293 cells were harvested 24 h after transfection and centrifuged; pellets were frozen at −80 °C. For co-immunoprecipitation experiments, cell pellets were thawed at room temperature and lysed in 5 volumes of extraction buffer (10 mM Hepes pH 7.9; 400 mM NaCl; 5% glycerol, PMSF 1 mM, leupeptin 0.5 mM, NaF 50 mM, pepstatin 1 mM). Samples were centrifuged at 34,000 rpm for 30 min at 4 °C, and supernatants were collected. Protein concentration was determined by the BCA assay (Pierce). Part of the lysate (20%) was kept as a positive input control. Lysates were incubated overnight with 10 μg of the indicated antibodies; 30 μl of protein G-Sepharose (GE Healthcare) were added for 4 h at 4 °C. The resin was washed five times with extraction buffer. Protein complexes were eluted by addition of sample buffer (Tris-Cl, 125 mM pH 6.8; 0.1 M 2-mercaptoethanol; 2% SDS; 20% glycerol; 25 mg/ml bromphenol blue), boiled for 15 min and separated on an 8% SDS-polyacrylamide gel. Proteins were transferred on a PVDF membrane (Millipore). Western blots were performed with the following antibodies: mouse anti-Myc (9E10, Santa Cruz Biotechnology), rabbit anti-Notch (C-20, Santa Cruz Biotechnology), rabbit anti-OAZ (ZFP423) (H-105 Santa Cruz Biotechnology), mouse anti-β-actin (Sigma). As secondary antibodies, a goat anti-rabbit HRP-conjugated antibody (Bio-Rad), and a

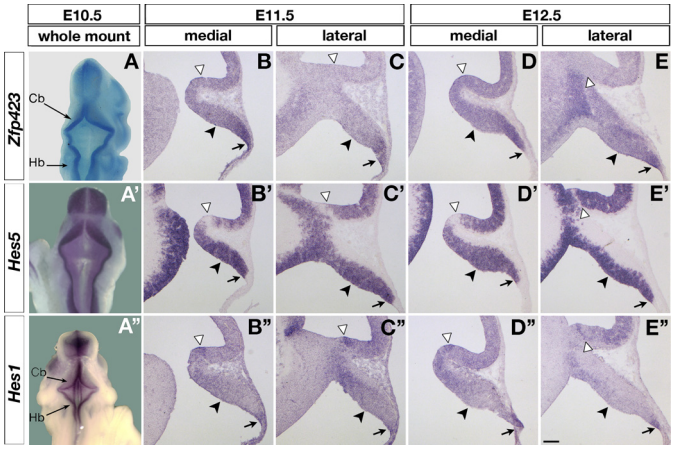

FIGURE 1. **Colocalization of *Zfp423* and *Hes5* in the medial cerebellar primordium.** *A*, whole mount LacZ staining of an E10.5 embryo carrying a gene trap insertion in the *Zfp423* locus. *A′* and *A″*, Whole mount E10.5 embryos hybridized with *Hes5* and *Hes1*, respectively. *Cb*, cerebellar primordium; *Hb*, hindbrain. Note *Zfp423* expression at the border with the roof plate. *B–E*, E11.5 and E12.5 sagittal sections from medial and lateral territories of the cerebellar primordium, hybridized with *Zfp423*. *Solid arrowhead*: VZ; *arrow*: RL. *B′–E′* and *B″–E″*) as above, hybridized with *Hes5* and *Hes1*, respectively. *Empty arrowhead* in B″ indicates the isthmic organizer (*IO*). Notably, *Hes5* is expressed in VZ and RL and sharply silenced in the IO, whereas *Hes1* is transcribed in the RL and IO, and silenced in most of the VZ.

sheep anti-mouse HRP-conjugated antibody (Amersham Biosciences) were used. Blots were developed with the LiteAblot substrate (EuroClone).

Statistical Analysis—Statistical significance was determined by the Student *t* test with a threshold for significance set to $p = 0.05$. All results are plotted as the mean ± S.D.

RESULTS

Zfp423 Expression in the Cerebellar Primordium—Because *Zfp423* mutants feature a severe cerebellar midline deletion (17, 19, 20), we re-examined the expression of *Zfp423* at the onset of cerebellar neurogenesis. To this end, we used a transgenic line (ID: W008G09, Ref. 38) carrying a *LacZ* gene inserted by gene trapping within the *Zfp423* gene. *Zfp423* expression in the neural plate is detectable by whole mount *in situ* hybridization as early as E7.5 (not shown). *Zfp423* strongly labels the rhombencephalon and mesencephalon at E8.5 and E9.5 (not shown, Ref. 17), and the hindbrain and cerebellum thereafter (Fig. 1*A*). *In situ* hybridization of embryonic tissue sections (Fig. 1, *B–E*) revealed that the gene is expressed in both germinative epithelia of the cerebellar primordium, *i.e.* the RL (*arrow*), that will give rise to all glutamatergic progenitors, and the cerebellar VZ (*solid arrowhead*), that harbors all GABAergic progenitors. Because *Zfp423* mutants feature a severe cerebellar midline deletion (17, 19, 20), we asked if the gene is expressed at this site (Fig. 1, *B* and *D*). Interestingly, in the E12.5 cerebellar primordium, *Zfp423* is expressed at high levels flanking the midline, where it colocalizes with *Hes5* (Fig. 1, *B′–D′*), an immediate transcriptional target of the Notch1 signaling pathway expressed in the VZ and RL. In contrast, *Hes1* is more restricted at this stage, labeling the isthmic organizer (*empty arrowhead*) and rhombic lip (*arrow*), adjacent to the cerebellar roof plate, while it is considerably down-regulated in most of the VZ (Fig. 1, *A″—E″*).

Functional and Molecular Interactions between ZFP423 and Notch Signaling—Based on the above observations, we sought to determine whether ZFP423 acts in the context of the Notch signaling pathway. To this end, we overexpressed the corresponding gene in neuralized P19 cells (see "Experimental Procedures") together with a cDNA encoding NICD (53). Shown in Fig. 2*A* is a sample semi-quantitative RT-PCR analysis of P19 cells transfected with a fixed amount of *Nicd* and increasing concentrations of *Zfp423*, illustrating the conditions achieved in subsequent experiments.

We measured the levels of four known direct targets of Notch signaling: *Hes5* and *Hes1* (12), *Nrarp* (54) and *Blbp* (55). As regards *Hes5* (Fig. 2*B*), whereas overexpression of *Nicd* alone produces a significant increase in *Hes5* gene expression over mock-transfected cells, the overexpression of *Zfp423* alone has no effect. However, combined overexpression of *Nicd* and *Zfp423* elicits a strong cooperative interaction, leading to a significant increase in *Hes5* transcript levels that is dependent on *Zfp423* DNA dosage. Likewise, *Blbp* gene expression (Fig. 2*C*) is cooperatively up-regulated by NICD and ZFP423, whereas *Hes1* and *Nrarp* transcript levels (Fig. 2, *D* and *E*, respectively) are unaffected by *Zfp423* overexpression in addition of *Nicd*. Because neuralized P19 cells express endogenous *Hes5* and *Zfp423* (Fig. 1*A* and Ref. 25), we moved to a system in which neither gene is expressed: the C2C12 myoblastoid cell line (25). In this system, overexpression of *Nicd* up-regulates *Hes1* and *Hey1* (56), but activates *Hes5* transcription very weakly (our observation). Our results indicate that in C2C12 cells *Hes5* expression is strictly dependent upon co-expression of *Nicd* and *Zfp423*, and that the levels of *Hes5* expression are again *Zfp423* dose-dependent (Fig. 2*F*). Next, we asked whether ZFP423 contributes to *Hes5* gene regulation even at physiological levels of expression. To address this point, we used RNA interference (RNAi). The efficiency of *Zfp423* knockdown was tested and validated at the protein level (supplemental Fig. S1). RNAs extracted from P19 cell lysates were analyzed by RT-qPCR for *Hes5* gene expression. In unstimulated P19 cells, transfected with a Zfp423 shRNA, *Hes5* transcription was clearly down-regulated (Fig. 2*G*). Next, we activated endogenous Notch signaling by growing P19 cells, transfected with the *Zfp423* shRNA, onto plates coated with a secreted form of the Notch ligand Jagged (Fc-Jagged) (51) or with an inactive control (Fc-TRAIL-R4). Our results indicated that in Jagged-activated P19 cells, *Hes5* is up-regulated (Fig. 2*H*), and that *Zfp423* RNAi causes a significant down-regulation of the same gene.

Next, we asked if the functional cooperation found to occur between ZFP423 and NICD also takes place *in vivo*. To address this question, we used *Xenopus laevis* neurula embryos. We identified a *Xenopus* expressed sequence tag clone (Image clone 6636947, GenBank™ accession: BU911031) very similar (83% identity at the nucleotide level) to *Gallus gallus ZFP423* (see "Experimental Procedures"). This clone was used as an *in situ* probe to analyze *Zfp423* distribution in neurula and tailbud stage embryos. The gene is expressed in the head and spinal cord (Fig. 3, *A* and *B*; see also stages 28 and 34 in supplemental Fig. S2). Subsequently, two-cell *Xenopus* embryos were injected unilaterally with mouse *Zfp423* and/or mRNA for *Xenopus Notch* ΔE (N^{act}); β-galactosidase

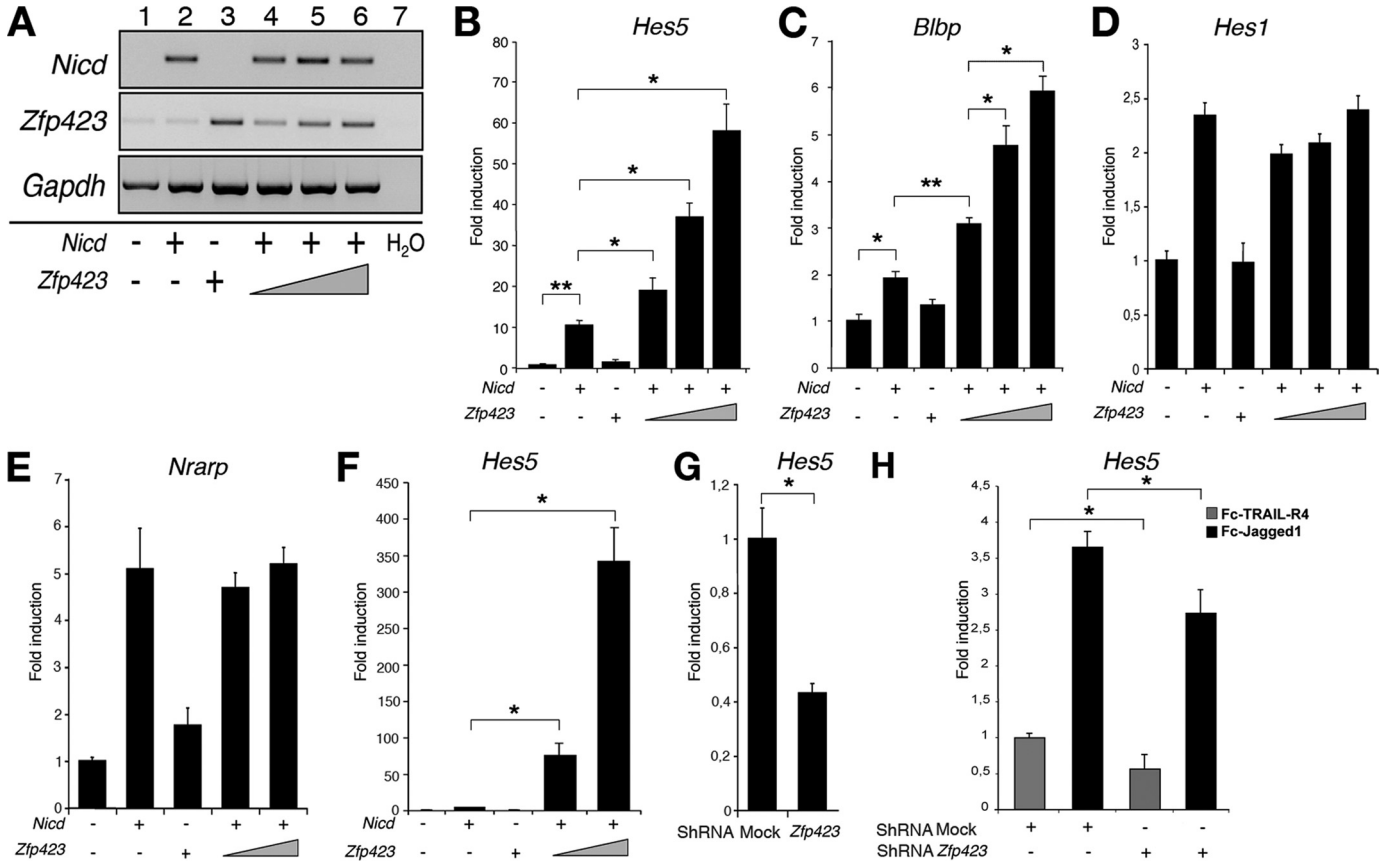

FIGURE 2. **Cooperative activation of *Hes5* and *Blbp* gene expression by NICD and ZFP423 in cell lines.** *A*, semiquantitative RT-PCR analysis of exogenous *Nicd* and *Zfp423* levels in transfected P19 cells. Note increasing *Zfp423* levels in *lanes 4–6*. This is representative of the amounts of *Nicd* and *Zfp423* cDNAs used in *B–F*. *B–G*, quantitative RT-PCR analysis of P19 (*B–E*, *G*) and C2C12 (*F*) cells treated as indicated below. *B* and *C*, *Nicd* and *Zfp423* coexpression in neuralized P19 cells up-regulates endogenous *Hes5* and *Blbp* expression, respectively, to a level greater than cells transfected with *Nicd* alone. Induction of *Hes5* and *Blbp* transcription is dependent on *Zfp423* dosage. *D* and *E*, cotransfection of P19 cells with *Nicd* and *Zfp423* fails to activate *Hes1* and *Nrarp* gene expression to a level greater than *Nicd* alone. *F*, transfection of C2C12 cells with *Nicd* and *Zfp423* induces *Hes5* gene expression in a *Zfp423* dose-dependent fashion. In this line, *Hes5* expression is strictly dependent on the addition of exogenous *Zfp423*. *G*, *Zfp423* RNA interference in P19 cells reduces endogenous *Hes5* expression. *H*, *Zfp423* RNA interference reduces *Hes5* expression in P19 cells grown on Fc-Jagged1-coated plates compared with cells plated onto Fc-TRAIL-R4-coated plates. *, $p \leq 0.05$; **, $p < 0.01$.

mRNA was included to mark the injected side. N^{act} encodes an N-terminally deleted, constitutively active *Xenopus* NOTCH protein (39). Both N^{act} and *Zfp423* mRNA concentrations were titrated so that either construct would produce moderate changes in target gene expression when overexpressed alone. As a first target, we analyzed the *Hes5* ortholog *ESR1* (57, 58). Our results (Fig. 3, *C–E*) indicate that embryos injected with *Zfp423* (600 pg) alone show a moderate activation of *ESR1* expression (Fig. 3*C*); likewise, injection of low amounts of N^{act} alone (100 pg) promoted a low-level expansion of the *ESR1* domain (Fig. 3*D*); however, the simultaneous overexpression of N^{act} (100 pg) and *Zfp423* (600 pg) sharply increased *ESR1* expression on the injected side (Fig. 3*E*). Furthermore, we asked whether the effect on *ESR1* expression produced by the injection of *Zfp423* alone (600 pg, Fig. 3*C*; 1 ng, Fig. 3*F*) requires endogenous Notch pathway activation. To address this question, *Zfp423* (1 ng) was coinjected with a dominant negative Delta ligand (DeltaStu, 40). $Delta^{Stu}$ coinjection ablated the expansion of *ESR1* consequent to *Zfp423* overexpression (Fig. 3*G*), indicating that this response is strictly dependent upon endogenous Notch signaling activation. Finally, we asked whether the endogenous expression of *ESR1* depends upon the presence of endogenous ZFP423. We injected 2-cell embryos with a ZFP423-specific morpholino antisense oligonucleotide and found a significant down-regulation of *ESR1* on the injected side (Fig. 3*H*) while the control morpholino had no effects on *ESR1* expression (Fig. 3*I*).

Because of the previously reported role of ZFP423 as a SMAD cofactor in the context of mesodermal patterning (25), the overexpression experiments were repeated by targeting unilaterally a dorsal blastomere at the 16-cell stage to prevent a possible interaction of exogenous ZFP423 with the BMP effector complex p-SMAD1-SMAD4 during gastrulation. The results of this experiment further corroborated the notion that *Zfp423* overexpression promotes *ESR1/Hes5* up-regulation on the injected side (Fig. 3*I*). In the same experiment, the *Hes1* ortholog *Hairy1* (10, 46) was either unchanged or slightly down-regulated on the injected side (Fig. 3*J*) and *Nrarp* (47, 54) transcript levels were also either left unchanged or slightly down-regulated (Fig. 3*K*) in response to *Zfp423* overexpression, indicating that *Zfp423* promotes a dissociation in the response to NICD *in vivo*, favoring the expression of *Hes5* over *Hes1* or other targets. Taken together, our *in vivo* results are consistent with those previously obtained in cell lines and point to a role

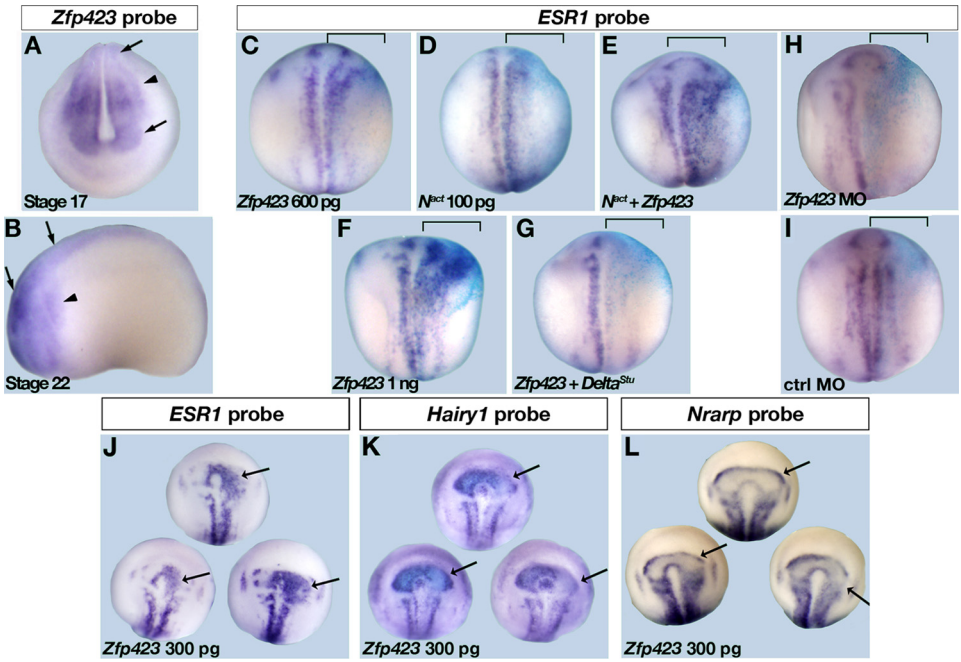

FIGURE 3. **Selective, cooperative activation of *ESR1* gene expression by N^{act} and ZFP423 in *Xenopus* embryos.** *A* and *B*, whole mount *in situ* hybridization analysis of *Xenopus Zfp423* gene expression in stage 17 (frontal view) and stage 22 (lateral view, head to the left) embryos, respectively: the gene is widely expressed starting in the neural plate/tube first (*arrow*), and then moving to the cranial neural crest (*arrowhead*). *C–E*, whole mount *in situ* hybridization analysis of *ESR1* gene expression in embryos injected unilaterally (*bracket*) with *Zfp423* (600 pg) and/or N^{act} (100 pg), as indicated. *LacZ* (*blue stain*) serves as an indicator of the injected side. Note strong *ESR1* expression after coinjection of N^{act} and *Zfp423*. *F*, embryo injected unilaterally (*bracket*) with 1 ng of *Zfp423*. *G*, embryo injected unilaterally (*bracket*) with 1 ng of *Zfp423* and 400 pg of $Delta^{Stu}$, encoding a dominant negative Notch ligand. Note disappearance of *ESR1* signal on the co-injected side. *H* and *I*, unilateral injection (*bracket*) of a *Zfp423* morpholino oligonucleotide (*H*) and of a control morpholino (*I*) (see "Experimental Procedures"). Note disappearance of *ESR1* signal on the injected side in embryos injected with *Zfp423*-specific morpholino unlike those injected with the control morpholino. *J–L*, *Zfp423* overexpression selectively up-regulates *ESR1* but not *Hairy1* or *Nrarp* in *Xenopus* embryos. Whole mount *in situ* hybridization analysis of *ESR1*, *Hairy1*, *and Nrarp* gene expression in embryos injected unilaterally with *Zfp423* (300 pg, *arrow*) in a dorsal blastomere. Note expanded *ESR1* expression domain (*J*), but reduced/unaffected expression of *Hairy1* (*K*) and *Nrarp* (*L*) on the injected side. *Gfp* was coinjected with *Zfp423* as a lineage tracer (not shown).

for *Zfp423* as a cell-autonomous modifier of Notch signal transduction.

Hes5 Promoter Analysis—To identify and map *Hes5* promoter sequences mediating the transcriptional response of *Hes5* to ZFP423 and NICD, we performed luciferase assays in C2C12 cells, using different extents of the *Hes5* 5′-flanking region, as described (61, 62). NICD binds to the *Hes5* promoter by forming a complex with CBF1/RBPjκ/CSL on a CBF1 recognition site (5), located 153 bp upstream of the murine *Hes5* ATG. At first, we used a luciferase (luc) reporter containing 1051 bp of the *Hes5* 5′-flanking sequence + 5′ UTR (sketched in Fig. 4*A*). Our results show that coexpression of *Nicd* and *Zfp423* leads to a significant (2-fold) increase in luc expression compared with *Nicd* alone (Fig. 4*A*). Similar results were obtained using a reporter construct containing a shorter stretch of the *Hes5* promoter/5′ UTR (267 bp) (Sketched in Fig. 4*B*), although the absolute activity levels were lower (Fig. 4*B*). These results indicate that while distal promoter regions contain elements that are important for *Hes5* gene activation, those regions are however not essential for the cooperation between NICD and ZFP423 to occur.

Next, we set out to establish whether ZFP423 interacts *in vivo* with the *Hes5* promoter. To this end, we performed a ChIP experiment using neuralized P19 cells (Fig. 4*C*) (see "Experimental Procedures"). P19 cell chromatin was immunoprecipitated using a ZFP423 Ab. For PCR amplification, we developed *Hes5* promoter-specific primers amplifying a 94-bp product spanning the BMP-responsive element (BRE) located within the *Hes5* promoter region depicted in Fig. 4*B*, an extremely GC-rich, PCR unfriendly sequence. We performed a qPCR using the *Hes5* primer pair and different control primers corresponding to an upstream 5′-flanking sequence (−2500 bp) and to two downstream sequences (+1600 bp and +2500 bp). In addition, we analyzed a syntenic gene (*Mrps15*) located megabases away from *Hes5* (63). The histogram in Fig. 4*C* shows a massive fold-enrichment for the *Hes5*-promoter-specific product with respect to flanking *Hes5* sequences and to the syntenic *Mrps15* gene.

Molecular Interactions between ZFP423 and NICD—Because our results indicated that *Zfp423* and *Nicd* cooperate functionally *in vitro* and *in vivo*, we investigated whether the corresponding proteins interact at the molecular level. First, COS7 cells were cotransfected with constructs encoding 6xmycZFP423 and flagNICD. Lysates were immunoprecipitated with an irrelevant anti-GFP, or with an anti-Myc monoclonal antibody. Immunoprecipitates were analyzed by WB using Abs for ZFP423 and for NICD, revealing an NICD-specific band only in the Myc-immunoprecipitated lane (Fig. 5*A*). To exclude the possibility that NICD might bind nonspecifically to the beads or the Myc antibody, the experiment was repeated, and lysates from single-transfected cells were immunoprecipitated as negative controls (Fig. 5*C*). NICD coimmunoprecipitated only in the cell lysates containing both factors.

EBF TF Overexpression Abolishes the Cooperation of ZFP423 with NICD—In previously published work (29), we showed that *Nicd* overexpression was capable of reducing or abolishing the ability of *XEbf2* to induce *Nfm* gene expression in *Xenopus* neurulas. This result suggested that Notch and EBF2 might act antagonistically in neuronal differentiation, through a mechanism independent of *Ebf2* gene transcription. Because ZFP423 is a molecular interactor of EBF TFs, we repeated the experiment described in Fig. 2*B* and added *Ebf1*, *Ebf2*, or *Ebf3* to the transfection mix. Transfected cells were harvested, lysed, and analyzed by RT-qPCR for *Hes5* mRNA levels. Our results indicate that *Ebf1–3* overexpression alone has no detectable effect on *Hes5* transcription. However, cotransfecting cells with *Nicd*,

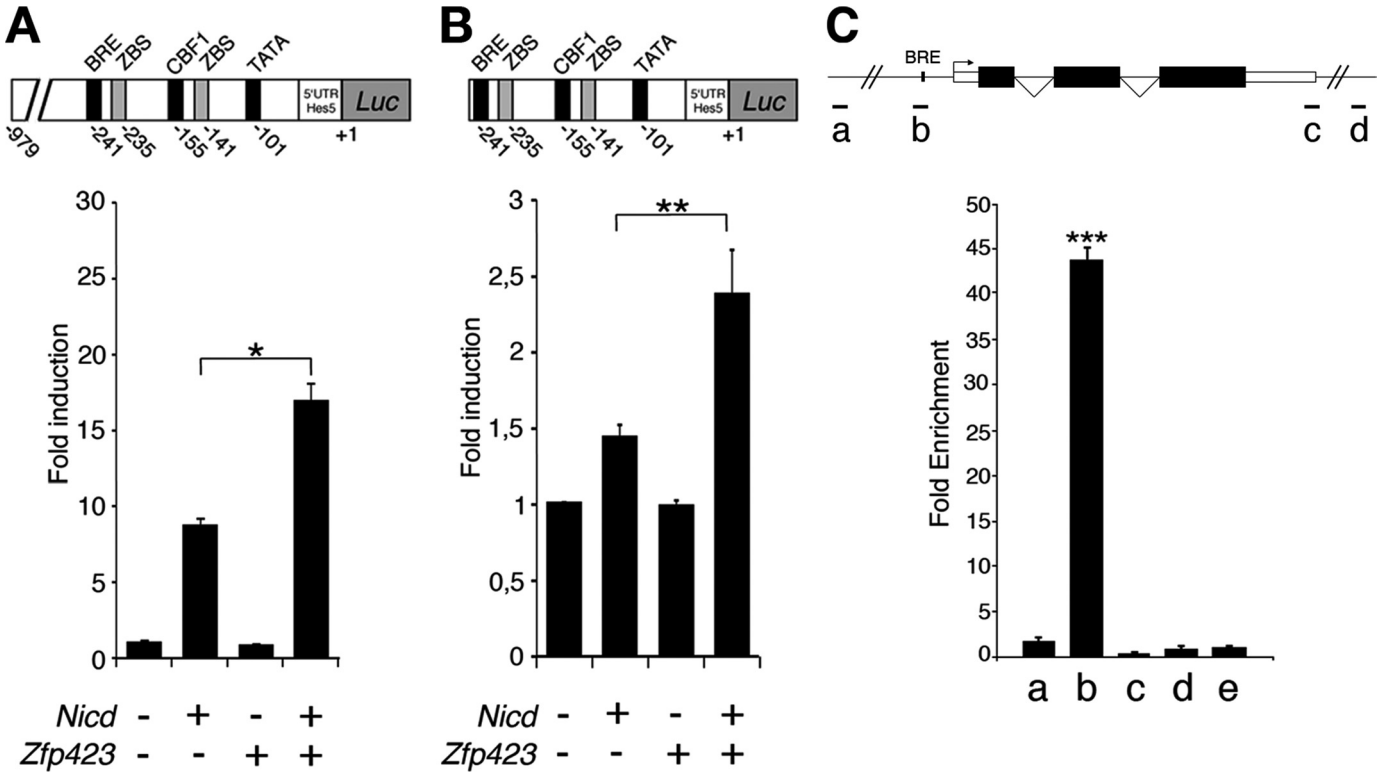

FIGURE 4. **ZFP423 binds to and activates the most proximal 267 bp of the Hes5 promoter.** *A* and *B*, promoter-reporter assays performed in C2C12 cells using a long and a short version of the *Hes5* gene promoter fused to luciferase. The two variants of the *Hes5* promoter are sketched above each histogram. *A*, 1-kb wt 5′-sequence responds to cotransfection with *Zfp423* by up-regulating luciferase compared with levels reached with *Nicd* alone. *B*, likewise, a 267-bp proximal element is cooperatively activated by *Nicd* and *Zfp423*, albeit to a lower level with respect to the experiment in *A*. *, $p < 0.05$; **, $p < 0.01$. *C*, chromatin immunoprecipitation was conducted on neuralized P19 cells. Sheared chromatin immunoprecipitated with anti-ZFP423 was purified and amplified by quantitative PCR. *a–d*, primer pairs spanning the *Hes5* gene (*b* is the primer pair spanning the BRE, see text). *e*, primer pair amplifying the syntenic gene *Mrps15*. Data are plotted as fold enrichment relative to the abundance of the *Mrps15* qPCR product (*e*). ***, $p < 0.0004$.

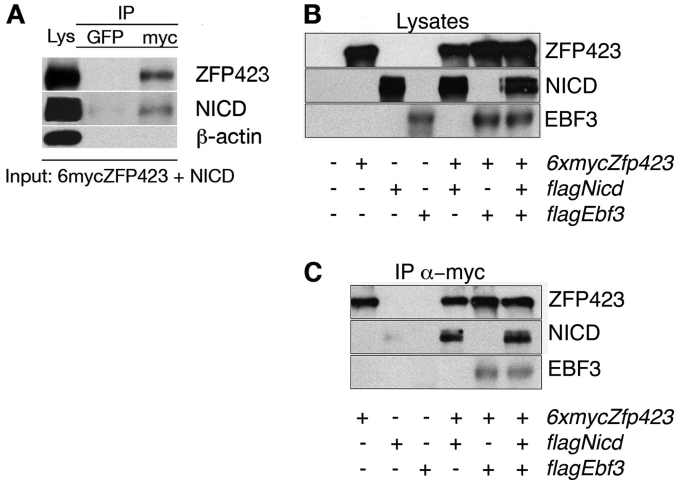

FIGURE 5. **Molecular interaction between ZFP423 and NICD.** In *A*, COS7 cells transfected with the indicated constructs, were subjected to immunoprecipitation using anti-GFP as an irrelevant antibody, or anti-Myc to precipitate 6xmycZFP423. Filters were cut and stained for ZFP423, NICD, and actin (unrelated protein). Only NICD coprecipitated in the fraction immunoprecipitated with anti-Myc. *B*, lysates of COS7 cells, transfected with the indicated constructs, were blotted and immunostained as shown. *C*, lysates shown in *B* were immunoprecipitated with the anti-Myc antibody. Filters were immunostained for ZFP423, NICD, and EBF3. Notably, NICD coprecipitated equally with ZFP423 in the presence or absence of EBF3.

Zfp423 and either *Ebf1*, *Ebf2*, or *Ebf3* antagonized the cooperative effect of ZFP423 and NICD on *Hes5* gene transcription (Fig. 6*A*). The experiment was repeated *in vivo*, by injecting 2-cell *Xenopus* embryos unilaterally with the same combination of mRNAs. Again, our *in vivo* results faithfully recapitulated those obtained in P19 cells: coinjection of either *XEbf2* (*C*) or *XEbf3* (Fig. 6*D*) reduced *ESR1* activation induced by exogenous *Zfp423* (Fig. 6*B*). *XEbf2* or *XEbf3* injection led to a low level of ectopic *ESR1* expression (Fig. 6, *E* and *F*). This might be caused by increased *X-Delta-1* expression, driven by XEBF2 (30) or to expression in differentiating neurons outside of the neural plate (28). Because our data indicate that EBFs interfere with the cooperation of ZFP423 and NICD, we asked if EBF overexpression can antagonize the assembly of the ZFP423-NICD molecular complex. To address this point, COS7 cells were cotransfected with 6xmycZFP423, flagNICD, and flagEBf3. Lysates were immunoprecipitated with anti-Myc and analyzed by WB using Abs for ZFP423, NICD and EBF3. Both NICD-specific and EBF specific bands were present in the anti-Myc immunoprecipitates (Fig. 5*C*). Again, lysates from single-transfected cells were used as negative controls. These results suggest that the three proteins form a complex exhibiting a reduced ability to activate *Hes5* gene expression.

Zfp423 Enhances the Cooperation between NICD and BMP/SMAD Signaling—Previous studies (25) showed that ZFP423 interacts with the SMAD1/SMAD4 complex in the nucleus to activate the *Xvent2* promoter in response to BMP signaling activation. Moreover, other authors have described the existence of interactions between BMP and Notch signaling pathways, resulting in repression of neurogenesis (61) and myogen-

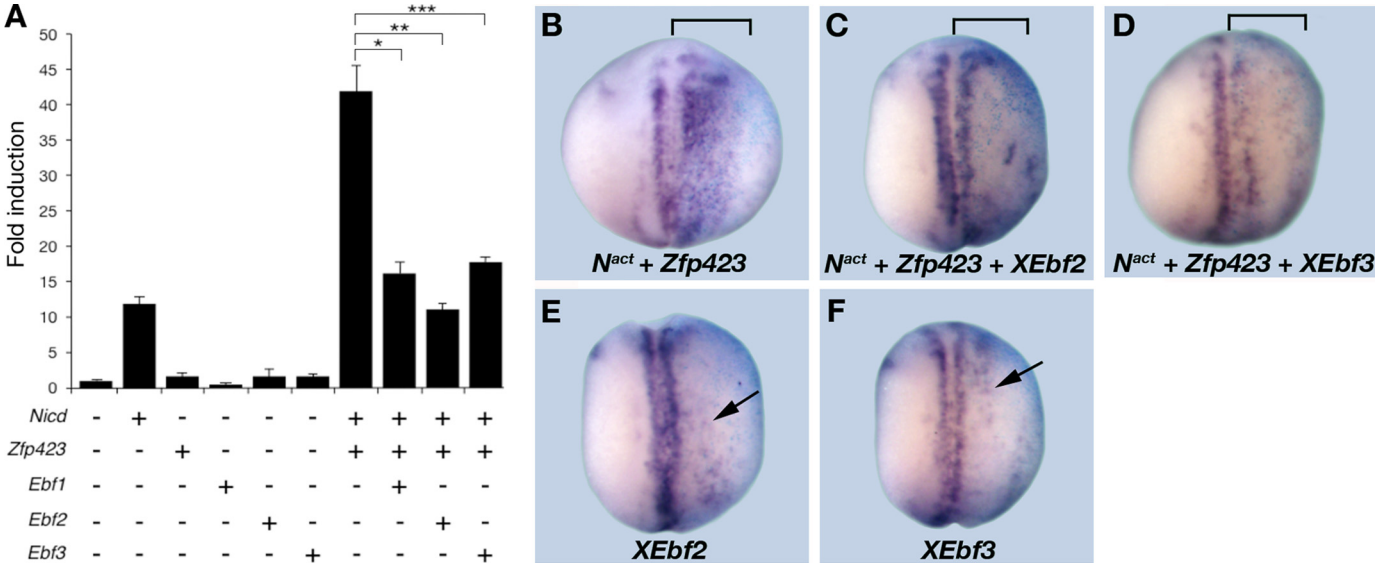

FIGURE 6. **EBF TFs reduce ZFP423-NICD-mediated *Hes5* gene expression *in vitro* and *in vivo*.** *A*, RT-qPCR analysis of *Hes5* gene expression in P19 cells transfected with the indicated constructs. Note that *Ebf1*, *Ebf2*, or *Ebf3* alone does not affect basal *Hes5* expression. *B–D*, whole mount *in situ* hybridization analysis of *ESR1* gene expression in embryos injected unilaterally (*bracket*) with N^{act} (100 pg) and *Zfp423* (600 pg) and/or *XEbf2* (100 pg) or *XEbf3* (100 pg). *E* and *F*, whole mount *in situ* hybridization analysis of *ESR1* gene expression in embryos injected unilaterally with *XEbf2* (100 pg) or *XEbf3* (100 pg), as indicated. Note slightly increased *ESR1*-positive cells in *XEbf2*- and *XEbf3*-injected embryos (*arrow*). *B–F*, *LacZ* (*blue stain*) serves as an indicator of the injected side.

esis (56), while others have proposed BMP as a rhombic lip (RL)-inducing signal in cerebellar development, antagonized by Notch signaling, which sets the RL ventral limit (64). Results obtained by other authors indicate that ZFP423 is a functional and molecular interactor of the SMAD1-SMAD4 complex. That interaction occurs thanks to a domain constituted by Zn fingers 9–20, encoded by exon 4 (25, 65). We asked if Zfp423 uses the same domain to interact with NICD. To address this question we generated a deleted construct missing Zn-fingers 9–20 (sketched in Fig. 7*A*). First, we overexpressed the construct in COS7 cells to determine the subcellular localization of the corresponding protein. Δ9–20 ZFP423 is expressed and displays a prevalent nuclear localization (Fig. 7*B*). Subsequently, we performed a promoter-reporter assay in C2C12 cells to compare the ability of wt and Δ9–20 ZFP423 to regulate *Hes5* gene expression. Our results indicate that Δ9–20 ZFP423 fails to cooperate with NICD in *Hes5* gene activation (Fig. 7*C*).

Because ZFP423 uses the same domain to interact functionally with both NICD and the SMAD complex, we asked whether and in which way ZFP423 might modulate the response of *Hes5* to BMP signaling activation (61). *In vivo*, *Zfp423* is expressed in the cerebellar primordium flanking the roof plate (Fig. 1*A*), a territory that expresses high levels of various BMP family molecules. To determine whether ZFP423 coordinates Notch- and BMP signaling recruiting both pathways in the activation of *Hes5* transcription, we performed an RT-qPCR experiment on mRNA extracted from C2C12 cells, measuring *Hes5* transcript levels in response to NICD and ZFP423, and in the presence or absence of purified BMP4 in the culture medium (Fig. 7*D*). To exclude the possibility that *Hes5* activation could stem from unequal expression levels of NICD in cells co-transfected with NICD and ZFP423 *versus* NICD alone, the levels of *Nicd* were analyzed by RT-qPCR and found to be virtually unchanged (Fig. 7*E*). Our results reproducibly indicate that, in the absence of ZFP423, a 2-h BMP treatment does up-regulate *Hes5* compared with the transcript levels achieved by transfecting the cells with *Nicd* alone. The interaction between BMP4 and NICD observed in C2C12 cells confirms the results reported by other authors (61). However, cotransfecting C2C12 with ZFP423 significantly potentiates (over 10-fold) the co-activating effect of BMP4 on NICD-induced *Hes5* gene expression (Fig. 7*D*), suggesting that this protein may play an important role integrating BMP and Notch signaling in dorsal territories of the neural tube.

DISCUSSION

ZFP423 Interacts Functionally and Molecularly with NICD to Activate Hes5 Gene Expression—In this report, we show that ZFP423 interacts functionally with the Notch intracellular domain to activate cooperatively and selectively the expression of one direct Notch target: *Hes5* (working model in Fig. 8). This effect occurs on a small stretch of *Hes5* proximal promoter, containing both a CBF1 binding site and a BMP responsive element. This interaction occurs *in vivo*, as shown by the results of ChIP experiments. However, ZFP423 has no noticeable effect on the expression of other NICD targets, such as *Hes1* or *Nrarp*. This conclusion is supported by experiments conducted both in cell lines and *Xenopus* embryos. The results of both gain-of-function and loss-of-function experiments, conducted *in vivo* and *in vitro*, support the notion that ZFP423 and NICD cooperate in *Hes5* regulation. Strikingly, in C2C12 cells, that are negative for both the *Hes5* and *Zfp423* transcripts, the expression of *Hes5* is strictly dependent upon the addition of exogenous *Zfp423*, as *Nicd* overexpression alone is not sufficient to activate it significantly, while it activates other Notch targets. This result suggests that ZFP423 acts selectively to recruit NICD onto the *Hes5* promoter.

ZFP423 May Coordinate BMP4 and Notch Signaling to Activate Hes5 Gene Expression Flanking the Dorsal Midline—Our results indicate that ZFP423, a known nuclear interactor of the BMP-dependent SMAD complex (25), acts to modulate the

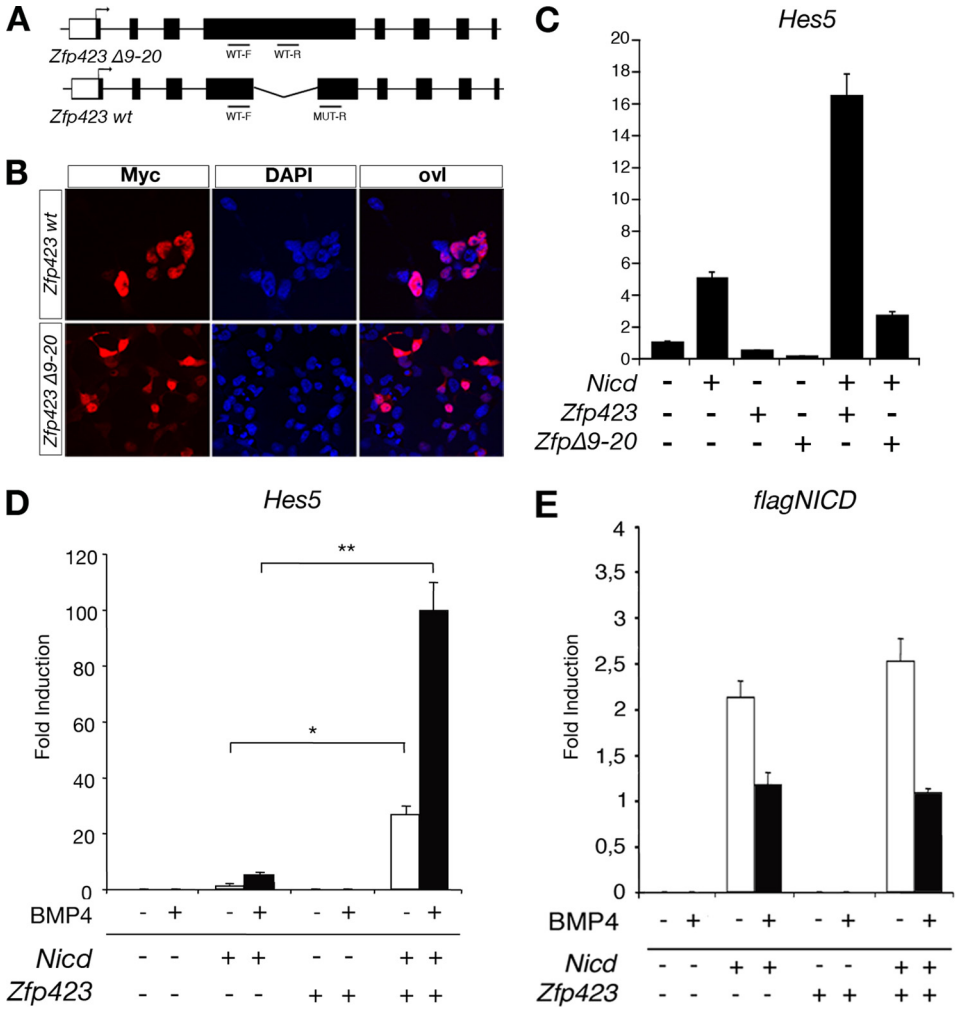

FIGURE 7. **ZFP423 cooperates with NICD and BMP signaling activation to promote *Hes5* gene expression.** Δ9–20 ZFP423 localizes partially in the cell nucleus but fails to activate *Hes5* gene expression in cooperation with NICD. *A*, scheme of the in-frame deletion of exon 4 producing a protein devoid of Zn fingers 9–20, implicated in the interaction with SMAD proteins and the BMP-responsive element. *B*, immunofluorescence analysis of the subcellular localization of a Myc-tagged wt and Δ9–20 construct in COS7 cells. Note that the mutant protein has a nuclear localization, although in some cells it is also distributed in the cytoplasm. DAPI labels DNA. *ovl*, overlay. *C*, histogram illustrating the results of a promoter-reporter assay revealing the lack of a cooperative interaction between Zfp423 Δ9–20 and NICD in *Hes5* gene activation. *D*, cooperative activation of *Hes5* gene expression by BMP4 and Notch mediated by ZFP423. Real-time RT-qPCR analysis of RNA from C2C12 cells, mock transfected or transfected with either *Nicd*, *Zfp423*, or both. Cells were either left untreated or treated with BMP4 for 2 h. Transfection with *Zfp423* strongly enhances the cooperative effect of NICD and BMP signaling on *Hes5* gene expression. *E*, RNAs from the C2C12 cell lysates analyzed in *D* were subjected to RT-qPCR using primers specific for flagNICD. FlagNICD expression levels are comparable in the presence and absence of Zfp423. This excludes the possibility that differences in *Hes5* expression depend on different levels of *flag-Nicd* in *Zfp423*-transfected *versus Zfp423*-untransfected samples. *, $p < 0.05$; **, $p < 0.005$.

function of NICD. The corresponding transcript, *Zfp423*, is expressed in two symmetric stripes of cells flanking the roof plate in the cerebellar primordium (present work, Fig. 1, and Ref. 21). Thus, we wondered if ZFP423 might integrate Notch signaling and roof plate signals cell autonomously to promote *Hes5* gene expression. Functional interactions between Notch and BMP signaling have been observed in urogenital and endothelial cells (59, 66), and BMP has been known to activate *Hes5* transcription mildly in mouse neuroepithelial cells (61), but the role of ZFP423 in this context was not examined. In C2C12 cells, we find that ZFP423 triggers a cooperative interaction between NICD and the SMAD complex, leading to a strong activation of *Hes5* gene expression. While this result could not be replicated in *Xenopus* embryos, because BMP activation in early embryos interferes with neural induction, *in vitro* studies reproducibly reveal that the cooperative interaction existing between NICD and the BMP pathway is enhanced by ZFP423 and results in *Hes5* up-regulation. For its cooperation with NICD (present work) and SMAD1/4 (25), ZFP423 uses the same domain, containing Zn fingers 9–20. This is a very large domain that likely accommodates both proteins permitting their cooperative rather than antagonistic interaction.

Previous reports have shown that *Zfp423* null mutants feature a disorganized cerebellar ventricular zone with disassembled radial glia. In neuralized P19 cells, ZFP423 regulates both *Hes5* and *Blbp* transcription in response to NICD. *In vivo*, *Hes5* transcription is strictly dependent upon Notch signaling activation and *Hes5* is expressed in asymmetrically dividing radial glia (12, 60). In the cerebellar primordium, *Hes5* labels the cerebellar VZ and rhombic lip, whereas *Hes1* is highly expressed in the rhombic lip and isthmic organizer, but is downregulated in most of the VZ (Fig. 1). We speculate that in dorsal territories of the cerebellar primordium the interaction occurring between Notch and BMP signaling, and enhanced by ZFP423, could maintain a pool of *Hes5*-positive radial glial progenitors supporting several rounds of asymmetric, neurogenic cell division, and prevent the premature occurrence of terminal differentiation. In keeping with this interpretation, expression of the radial glia marker BLBP has been found reduced in *Zfp423* mutants (20).

EBF TFs Antagonize the ZFP423-NICD-mediated Activation of Hes5 Gene Expression—The cooperative interaction established by ZFP423 and NICD can be quenched by cotransfecting cells with cDNAs encoding TFs of the EBF ^{COE} family. EBF TFs also block the cooperative interaction between ZFP423 and N^{act} in *Xenopus* embryos. EBF TFs have been implicated in neuronal differentiation, and ZFP423 acts as an EBF antagonist both in promoter-reporter assays (26) and, *in vivo*, in olfactory neurogenesis (23). The reported ability of ZFP423 to block differentiation when expressed ectopically in postmitotic precur-

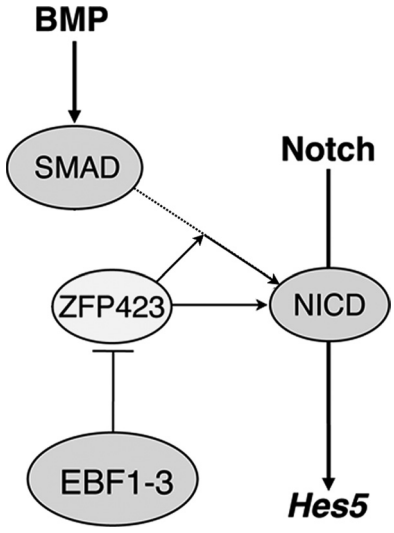

FIGURE 8. **A working model of the interactions between ZFP423 and other networks in *Hes5* gene activation.** *Hes5* expression is induced upon Notch signaling activation independently of ZFP423. ZFP423 boosts the effect of Notch signaling by forming a complex with NICD and by recruiting it onto the *Hes5* promoter. The interaction between the BMP4 transducer SMAD1-SMAD4 and ZFP423 further potentiates this effect (*solid arrow*), although BMP4 signaling might also cooperate with NICD in the absence of ZFP423 (*stippled arrow*). In overexpression experiments, EBF/COE transcription factors antagonize *Hes5* activation by competing with NICD for the interaction with ZFP423.

sors, and to revert them to an undifferentiated state, could be explained partially by the ability, shown here, of ZFP423 to promote *Hes5* gene expression. Conversely, the ability of EBF TFs to couple cell cycle exit to the onset of differentiation may stem in part from recruiting ZFP423 into molecular processes other than its cooperation with Notch signaling. In other words, EBF TFs may compete with NICD for ZFP423 in differentiating radial progenitors, and recruit ZFP423 in neuronal differentiation and migration (28). Our co-immunoprecipitation results indicate that EBF3 does not interfere significantly with the assembly of a ZFP423-NICD complex, thus suggesting that the presence of EBF TFs may recruit NICD and ZFP423 into a distinct regulatory network, sequestering it from the *Hes5* promoter.

In summary, ZFP423 synergizes with NICD and cell-autonomously integrates BMP signaling with the Notch pathway, leading to the selective up-regulation of one direct target of Notch: *Hes5*. By doing so, *Zfp423* may promote the maintenance of an undifferentiated radial glial progenitor pool. *In vivo* gain-of-function studies are now required to fully elucidate the roles of Zfp423 in the context of cerebellar neurogenesis.

REFERENCES

1. Artavanis-Tsakonas, S., Rand, M. D., and Lake, R. J. (1999) *Science* **284,** 770–776
2. Kageyama, R., Ohtsuka, T., Shimojo, H., and Imayoshi, I. (2008) *Nat. Neurosci.* **11,** 1247–1251
3. Brou, C., Logeat, F., Gupta, N., Bessia, C., LeBail, O., Doedens, J. R., Cumano, A., Roux, P., Black, R. A., and Israël, A. (2000) *Mol. Cell* **5,** 207–216
4. Mumm, J. S., Schroeter, E. H., Saxena, M. T., Griesemer, A., Tian, X., Pan, D. J., Ray, W. J., and Kopan, R. (2000) *Mol. Cell* **5,** 197–206
5. Jarriault, S., Brou, C., Logeat, F., Schroeter, E. H., Kopan, R., and Israel, A. (1995) *Nature* **377,** 355–358
6. Hsieh, J. J., Zhou, S., Chen, L., Young, D. B., and Hayward, S. D. (1999) *Proc. Natl. Acad. Sci. U.S.A.* **96,** 23–28
7. Wu, L., Aster, J. C., Blacklow, S. C., Lake, R., Artavanis-Tsakonas, S., and Griffin, J. D. (2000) *Nat. Genet.* **26,** 484–489
8. Fryer, C. J., Lamar, E., Turbachova, I., Kintner, C., and Jones, K. A. (2002) *Genes Dev.* **16,** 1397–1411
9. Wallberg, A. E., Pedersen, K., Lendahl, U., and Roeder, R. G. (2002) *Mol. Cell Biol.* **22,** 7812–7819
10. Jennings, B., Preiss, A., Delidakis, C., and Bray, S. (1994) *Development* **120,** 3537–3548
11. Sasai, Y., Kageyama, R., Tagawa, Y., Shigemoto, R., and Nakanishi, S. (1992) *Genes Dev.* **6,** 2620–2634
12. Ohtsuka, T., Ishibashi, M., Gradwohl, G., Nakanishi, S., Guillemot, F., and Kageyama, R. (1999) *EMBO J.* **18,** 2196–2207
13. Hatakeyama, J., Bessho, Y., Katoh, K., Ookawara, S., Fujioka, M., Guillemot, F., and Kageyama, R. (2004) *Development* **131,** 5539–5550
14. Kageyama, R., Ohtsuka, T., and Kobayashi, T. (2007) *Development* **134,** 1243–1251
15. Kadesch, T. (2004) *Curr. Opin. Genet. Dev.* **14,** 506–512
16. Bray, S. J. (2006) *Nat. Rev.* **7,** 678–689
17. Cheng, L. E., Zhang, J., and Reed, R. R. (2007) *Dev. Biol.* **307,** 43–52
18. Chizhikov, V. V., Lindgren, A. G., Currle, D. S., Rose, M. F., Monuki, E. S., and Millen, K. J. (2006) *Development* **133,** 2793–2804
19. Warming, S., Rachel, R. A., Jenkins, N. A., and Copeland, N. G. (2006) *Mol. Cell Biol.* **26,** 6913–6922
20. Alcaraz, W. A., Gold, D. A., Raponi, E., Gent, P. M., Concepcion, D., and Hamilton, B. A. (2006) *Proc. Natl. Acad. Sci. U.S.A.* **103,** 19424–19429
21. Cheng, L. E., Zhang, J., and Reed, R. R. (2007) *Dev. Biol.* **307,** 43–52
22. Millen, K. J., and Gleeson, J. G. (2008) *Curr. Opin. Neurobiol.* **18,** 12–19
23. Cheng, L. E., and Reed, R. R. (2007) *Neuron* **54,** 547–557
24. Liu, A., and Niswander, L. A. (2005) *Nat. Rev. Neurosci.* **6,** 945–954
25. Hata, A., Seoane, J., Lagna, G., Montalvo, E., Hemmati-Brivanlou, A., and Massagué, J. (2000) *Cell* **100,** 229–240
26. Tsai, R. Y., and Reed, R. R. (1997) *J. Neurosci.* **17,** 4159–4169
27. Tsai, R. Y., and Reed, R. R. (1998) *Mol. Cell Biol.* **18,** 6447–6456
28. Garcia-Dominguez, M., Poquet, C., Garel, S., and Charnay, P. (2003) *Development* **130,** 6013–6025
29. Pozzoli, O., Bosetti, A., Croci, L., Consalez, G. G., and Vetter, M. L. (2001) *Dev. Biol.* **233,** 495–512
30. Dubois, L., Bally-Cuif, L., Crozatier, M., Moreau, J., Paquereau, L., and Vincent, A. (1998) *Curr. Biol.* **8,** 199–209
31. Corradi, A., Croci, L., Broccoli, V., Zecchini, S., Previtali, S., Wurst, W., Amadio, S., Maggi, R., Quattrini, A., and Consalez, G. G. (2003) *Development* **130,** 401–410
32. Wang, M. M., and Reed, R. R. (1993) *Nature* **364,** 121–126
33. Davies, J. A., and Reed, R. (1996) *J. Neurosci.* **16,** 5082–5094
34. Wang, S. S., Tsai, R. Y., and Reed, R. R. (1997) *J. Neurosci.* **17,** 4149–4158
35. Croci, L., Chung, S. H., Masserdotti, G., Gianola, S., Bizzoca, A., Gennarini, G., Corradi, A., Rossi, F., Hawkes, R., and Consalez, G. G. (2006) *Development* **133,** 2719–2729
36. Chung, S. H., Marzban, H., Croci, L., Consalez, G. G., and Hawkes, R. (2008) *Neuroscience* **153,** 721–732
37. Huang, S., Laoukili, J., Epping, M. T., Koster, J., Hölzel, M., Westerman, B. A., Nijkamp, W., Hata, A., Asgharzadeh, S., Seeger, R. C., Versteeg, R., Beijersbergen, R. L., and Bernards, R. (2009) *Cancer Cell* **15,** 328–340
38. Skarnes, W. C., von Melchner, H., Wurst, W., Hicks, G., Nord, A. S., Cox, T., Young, S. G., Ruiz, P., Soriano, P., Tessier-Lavigne, M., Conklin, B. R., Stanford, W. L., and Rossant, J. (2004) *Nat. Genet.* **36,** 543–544
39. Coffman, C. R., Skoglund, P., Harris, W. A., and Kintner, C. R. (1993) *Cell* **73,** 659–671
40. Chitnis, A., Henrique, D., Lewis, J., Ish-Horowicz, D., and Kintner, C. (1995) *Nature* **375,** 761–766
41. Chalfie, M., Tu, Y., Euskirchen, G., Ward, W. W., and Prasher, D. C. (1994) *Science* **263,** 802–805
42. Nieuwkoop, P. D., and Faber, J. (1967) *Normal Table of Xenopus laevis*, North Holland Publishing Company, Amsterdam, The Netherlands
43. Harland, R. M. (1991) in *Xenopus laevis: Practical Uses in Cell and Molecular Biology* (Kay, B. K., and Peng, H. B., eds), Academic Press, San Diego

44. Turner, D. L., and Weintraub, H. (1994) *Genes Dev.* **8,** 1434–1447
45. Wettstein, D. A., Turner, D. L., and Kintner, C. (1997) *Development* **124,** 693–702
46. Dawson, S. R., Turner, D. L., Weintraub, H., and Parkhurst, S. M. (1995) *Mol. Cell Biol.* **15,** 6923–6931
47. Lamar, E., Deblandre, G., Wettstein, D., Gawantka, V., Pollet, N., Niehrs, C., and Kintner, C. (2001) *Genes Dev.* **15,** 1885–1899
48. Vincent, V. A., DeVoss, J. J., Ryan, H. S., and Murphy, G. M., Jr. (2002) *J. Neurosci. Res.* **69,** 578–586
49. Jensen, J., Pedersen, E. E., Galante, P., Hald, J., Heller, R. S., Ishibashi, M., Kageyama, R., Guillemot, F., Serup, P., and Madsen, O. D. (2000) *Nat. Genet.* **24,** 36–44
50. Lowell, S., Benchoua, A., Heavey, B., and Smith, A. G. (2006) *PLoS Biol.* **4,** e121
51. Buas, M. F., Kabak, S., and Kadesch, T. (2009) *J. Cell Physiol.* **218,** 84–93
52. Ausubel, F. M., Brent, R., Kingstone, R. E., Moore, D. D., Smith, J. A., and Struhl, K. (1995) *Curr. Prot. Mol. Biol.*, J. Wiley and Sons, New York
53. Schroeter, E. H., Kisslinger, J. A., and Kopan, R. (1998) *Nature* **393,** 382–386
54. Krebs, L. T., Deftos, M. L., Bevan, M. J., and Gridley, T. (2001) *Dev. Biol.* **238,** 110–119
55. Anthony, T. E., Mason, H. A., Gridley, T., Fishell, G., and Heintz, N. (2005) *Genes Dev.* **19,** 1028–1033
56. Dahlqvist, C., Blokzijl, A., Chapman, G., Falk, A., Dannaeus, K., Ibâñez, C. F., and Lendahl, U. (2003) *Development* **130,** 6089–6099
57. Davis, R. L., and Turner, D. L. (2001) *Oncogene* **20,** 8342–8357
58. Lamar, E., and Kintner, C. (2005) *Development* **132,** 3619–3630
59. Itoh, F., Itoh, S., Goumans, M. J., Valdimarsdottir, G., Iso, T., Dotto, G. P., Hamamori, Y., Kedes, L., Kato, M., and ten Dijke, Pt., P. (2004) *EMBO J.* **23,** 541–551
60. Ohtsuka, T., Sakamoto, M., Guillemot, F., and Kageyama, R. (2001) *J. Biol. Chem.* **276,** 30467–30474
61. Takizawa, T., Ochiai, W., Nakashima, K., and Taga, T. (2003) *Nucleic Acids Res.* **31,** 5723–5731
62. Ohtsuka, T., Imayoshi, I., Shimojo, H., Nishi, E., Kageyama, R., and McConnell, S. K. (2006) *Mol. Cell. Neurosci.* **31,** 109–122
63. Henke, R. M., Savage, T. K., Meredith, D. M., Glasgow, S. M., Hori, K., Dumas, J., MacDonald, R. J., and Johnson, J. E. (2009) *Development* **136,** 2945–2954
64. Machold, R. P., Kittell, D. J., and Fishell, G. J. (2007) *Neural. Dev.* **2,** 5
65. Ku, M., Howard, S., Ni, W., Lagna, G., and Hata, A. (2006) *J. Biol. Chem.* **281,** 5277–5287
66. Grishina, I. B., Kim, S. Y., Ferrara, C., Makarenkova, H. P., and Walden, P. D. (2005) *Dev. Biol.* **288,** 334–347
67. Chitnis, A., and Kintner, C. (1996) *Development* **122,** 2295–2301
68. Croci, L., Barili, V., Chia, D., Massimino, L., van Vugt, R., Masserdotti, G., Rotwein, P., and Consalez, G. G. (2010) *Cell Death Differ.*, in press